Invited Articles

Liquid fraction profile in a liquid foam under an applied voltage

Anne-Laure Biance* and Oriane Bonhomme
Univ Lyon, Université Claude Bernard Lyon 1, CNRS, Institut Lumière Matière, F-69622 Villeurbanne, France

(Received 29 June 2018; published 21 November 2018)

A liquid foam, a dense assembly of gas bubbles in a surfactant solution, is a deformable porous material. As classically observed in divided systems, electrokinetic transport can be induced, for example, when an electric field is applied from either side of the foam sample. We determine here the liquid fraction profile obtained when a foam is submitted to an electro-osmotic flow, when the surfactant induces so-called rigid or mobile interfaces. We show that the main governing equation for the liquid fraction repartition in space and time is diffusivelike and similar to the one describing pressure-induced drainage only. The electric field however significantly affects the general profile by modifying the boundary conditions. A capillary number that compares electro-osmotic stress and capillary pressure in the foam geometry is introduced and characterizes the magnitude of electrically induced flow in a macroscopic foam. In particular, the ability of a foam to capture liquid from a reservoir is quantitatively estimated.

DOI: 10.1103/PhysRevFluids.3.110505

I. INTRODUCTION

The experimental demonstration of electro-osmotic flows dates back to two pioneering experiments of Reuss [1]. The first one consists of applying a difference of voltage at the extremities of an assembly of quartz grains contained in a tube and plunged in an electrolyte solution, as represented in Fig. 1. After a few days, a displacement of the liquid level is observed. We note that this experiment was carried out just after the discovery of the first chemical battery by Volta, consisting of a pile of copper and zinc disks embedded in an electrolytic solution, as represented in Fig. 1. From this particular shape, a chemical battery is still called *pile* in French.

Subsequently, the effect of electrokinetics on transport properties at the nanoscale was thoroughly studied in the seminal work of Smoluchowski [2] and then extensively, for example, in a series of papers by Elton [3–5]. Even if it is an old topic, investigations are limited by the difficulty to design well-controlled systems at the nanoscale. However, these studies have regained interest, adapting well-characterized fabrication techniques, previously developed for the microelectronics industry [2,6]. From this, different types of actuation and coupled transport properties have been investigated in nanofluidic systems, with the goal of identifying the functionalities which can best enhance these properties at low cost.

These transport properties can be described by the linear response theory and characterized by the symmetrical Onsager matrix [7] defined as

$$\begin{pmatrix} Q \\ I \\ J_T \\ \vdots \end{pmatrix} = \mathcal{A} \times \begin{bmatrix} L_H & \alpha & \alpha_{\text{th}} & \cdots \\ \alpha & G & \beta_{\text{th}} & \cdots \\ \alpha_{\text{th}} & \beta_{\text{th}} & G_{\text{th}} & \cdots \\ \cdots & \cdots & \cdots & \cdots \end{bmatrix} \times \begin{pmatrix} -\nabla P \\ -\nabla U \\ -\frac{\nabla T}{T} \\ \vdots \end{pmatrix}, \tag{1}$$

*Anne-Laure.biance@univ-lyon1.fr

 ©2018 American Physical Society

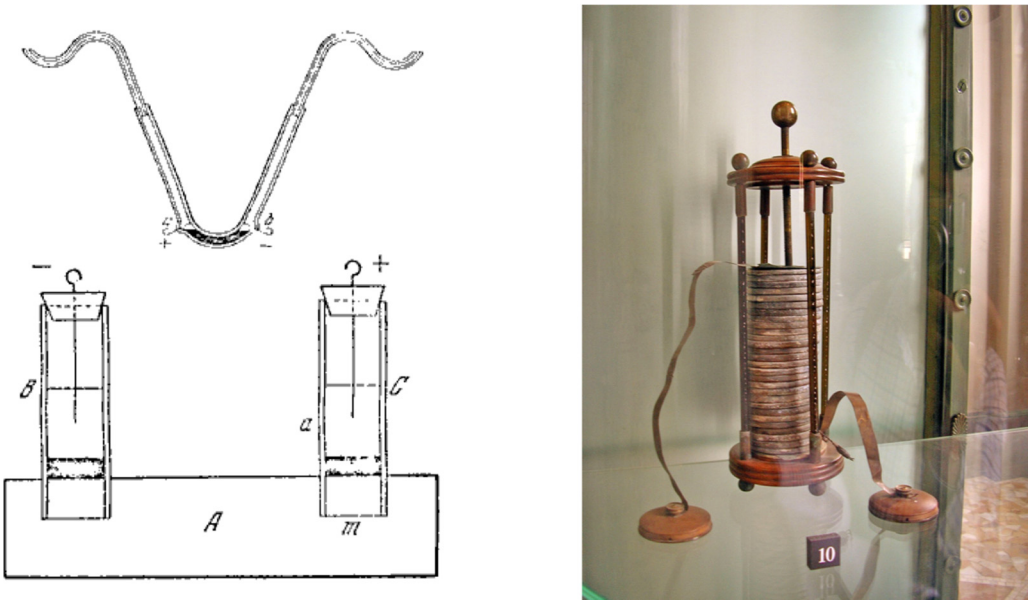

FIG. 1. Shown on the left is the scheme of the experiments performed by Reuss, which shows an electro-osmotic flow [1]. On the right is a picture of a reproduction of the Volta battery.

where Q is the matter flux, I the electric current, J_T the heat flux, P the pressure, U the voltage, and T the temperature. The different terms of the Onsager matrix will be elaborated on below.

The nondiagonal terms of the matrix account for interactions of the liquid with the surfaces. Though second order, they are of course of larger magnitude in large-surface-area systems, for example, confined at the nanoscale. The values of these terms and especially the intricate coupling existing between hydrodynamic and static interactions with a surface are still active subjects of research [6] at the interface between surface chemistry, nonequilibrium physics, and fluid mechanics. We will consider here nanofluidic transport in a macroscopic soft divided system in a liquid foam.

The article is organized as follows. First, we underline some specifics of foamy materials that could affect coupled transport and give a short review of experiments performed in these systems. We then focus on the specific case of electrokinetic transport and determine how the distribution of liquid in a foam is affected by the presence of an electric field. To do that, we present general equations allowing us to define everywhere the liquid fraction in a foam sample. As it has been performed for mass transport or so-called foam drainage, we will then consider two distinct cases depending on the nature of the foam. In each case, two geometries, an isolated foam or a foam in contact with a reservoir, will be considered.

II. SPECIFICITIES OF TRANSPORT IN A LIQUID FOAM

A. Complex poroelastic medium with fluidic interfaces

1. Foam geometry

A liquid foam consists of a dispersion of gas bubbles in a liquid matrix. An important characteristic of the material is its liquid fraction ϕ, defined as the ratio of the volume of liquid to the total volume of the foam. This parameter is used to distinguish bubbly liquids (typically for $\phi \geqslant 30\%$) from wet foams (typically $\phi \geqslant 15\%$) and dry foams ($\phi \leqslant 5\%$) [8]. In dry foams, bubbles are in contact and display a polyhedric shape (we then talk of a Kelvin structure) due to Plateau's

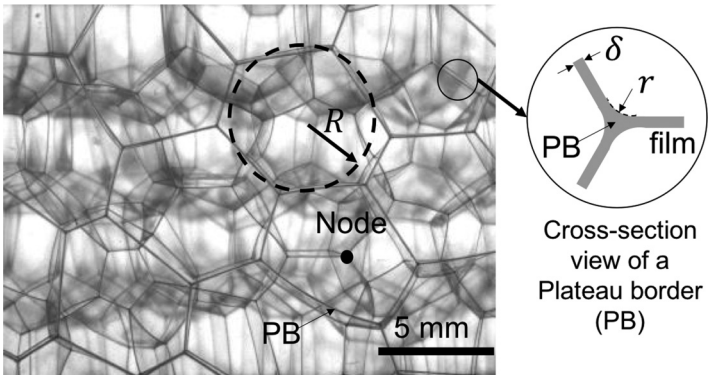

FIG. 2. Image of a liquid foam to identify its structural elements. The Plateau borders are small liquid channels that link three films, as represented in the cross section, and the nodes are at the junction of four PBs. Here R is the typical radius of a bubble.

law. In wet foams, bubbles stay spherical with a large amount of liquid in between. At a liquid fraction above $\phi_r = 26\%$ (random close packing liquid fraction for dense monodisperse ordered systems), the bubbles are no longer in contact and the system is considered a continuous liquid.

As shown in Fig. 2, a liquid foam has a multiscale structure and it is crucial to take into account the different scales when studying the transport in such a material. The first macroscopic scale is the size of the foam sample, labeled L. On the length scale of individual bubbles, one has to take into account the bubble radius R that can vary from few hundreds of micrometers to centimeters in usual systems. Note that when bubbles are not spherical, this radius corresponds to the one of a spherical bubble of identical volume. The thin flat films separating two bubbles, often colored because of light interference, have a typical thickness δ of 0.1 μm. Three films join at 120°, following Plateau rules [8], in a liquid channel called a Plateau border (PB). The PB's length and radius of curvature are denoted by ℓ and r, respectively. Four PBs join in a node. As we will focus here on a macroscopic description, we omit the scale of the surfactants, subnanometric, whose presence is crucial to stabilize a soap film or a liquid foam.

The arrangement of bubbles can be ordered or disordered, mainly because of the bubble radius polydispersity. In monodisperse systems, different arrangements have been observed, depending on the boundary imposed arrangement [9] or on the liquid fraction [10]. In the following, the transport coefficients of the Onsager matrix are usually defined under the hypothesis that the foam structure is a Kelvin structure [8], sketched in Fig. 3.

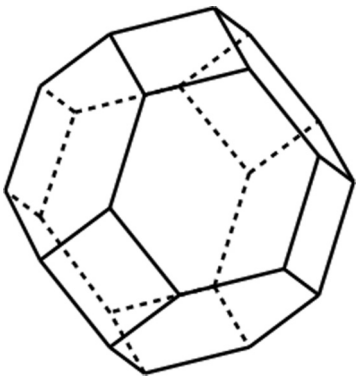

FIG. 3. Scheme of the unit cell (one bubble) of a Kelvin structure [8].

2. Hydrodynamic boundary condition

Mass transport, whether it is coupled to other actuations (thermo-osmotic, electrokinetic, diffusio-osmotic, etc.) or not (pressure-driven drainage in liquid foam) depends not only on specific interfacial properties but also on the hydrodynamic boundary conditions in such systems [2,8,10–15]. When a liquid-gas interface, covered with surfactants, is considered, one has to take into account two boundary conditions: the motion of the liquid with respect to the surfactant layer and the motion of the surfactants in the laboratory frame [14].

Considering the relative motion of the liquid versus the surfactant layer, it may be defined by a finite friction coefficient or by a slip length [16], defined as $b = -\frac{1}{v_t}\frac{\partial v_t}{\partial n}$, with t and n the tangent and the normal to the interface, respectively, and v_t the tangential relative velocity between the liquid and the surfactants. To define the influence of the slippage on the flow rate in a confined geometry, one has to compare the slip length to the lateral dimension of the channel. In the case of soap films, this slip length has been characterized by molecular dynamic simulations [17] in the case of a common anionic surfactant (sodium dodecyl sulfate) and varies as the inverse of the surface concentration (the more surfactants, the larger the friction and the smaller the slip length). Quantitatively, at surface concentrations for which we can form a stable film or foam (fully covered interfaces), the slip length is of the order of 0.1–0.2 nm [17] and so is definitely negligible in realistic experimental conditions.

The second boundary condition concerns the motion of the surfactants with respect to the laboratory frame and in particular their ability to distribute inhomogeneously along the interface and generate surface tension gradients and subsequent so-called Marangoni stresses [8]. The possible generation of these stresses depends first on the situation considered. Whereas it has been shown to be crucial when considering foam drainage [10,18] or thermo-osmosis [13,19], it is less relevant in the specific case of electro-osmosis. Indeed, in this particular situation, it has been shown theoretically and experimentally [14] that no force is acting on the surfactants: The viscous friction associated with the flow is directly compensated by the electric force on the surfactants [20,21].

For simplification, since it often corresponds to distinct well-defined experimental situations, two extreme cases of rigid and mobile interfaces are typically considered [22]. Rigid interfaces correspond to a vanishing velocity at the liquid-air interface, whereas mobile interfaces correspond to a stress-free condition at the liquid-gas boundary. The surface rigidity is currently a subject of active research [10] and describing it quantitatively requires the introduction of surface viscoelasticity moduli and an analysis of the microscopic origins of surface dissipation. It is generally admitted that the regime observed mainly depends on the surfactant type used to stabilize the foam. However, one has to be cautious as the same formulation of a foam can lead to a rigidlike interface behavior or a mobile one, depending on the foam geometry, the actuation type, or magnitude.

3. Elasticity of the foam

A foam is a deformable porous material. The pressure inside the foam which describes its ability to absorb liquid when in contact with a semipermeable membrane is known in the community as osmotic pressure. It has been extensively investigated [23,24] and depends on the foam structure (ordered or disordered mainly) and its liquid fraction. We will consider here only the pressure in the liquid, which we will approximate as the capillary pressure within the foam and, in the case of dry foam [23], is given by $\Delta P \simeq -\gamma/r$, where γ is the interfacial tension and r is the radius of curvature of the Plateau borders. If we consider that most of the liquid is located in the Plateau borders (we neglect the volume of the nodes and of the films [8]), the pressure in the liquid is then linked to the liquid fraction ϕ as

$$\Delta P = -\beta \frac{\gamma}{R}\frac{1}{\sqrt{\phi}}, \tag{2}$$

where β is a geometrical factor equal to 1.715 for a Kelvin structure [8]. In the following, we will generally consider the pressure gradient in the vertical direction x, defined in Fig. 4 and derived

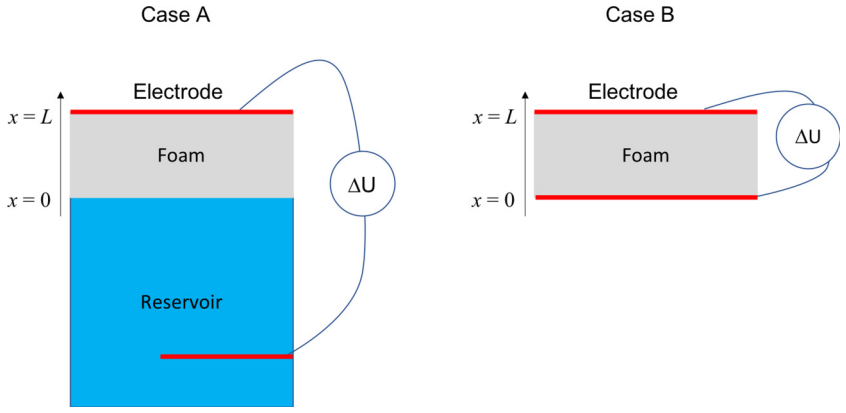

FIG. 4. Scheme of the two cases considered. In case A the foam is in contact with a liquid reservoir. One electrode is in the reservoir, the other one is at the top of the foam. In case B the foam is squeezed between two electrodes and isolated from the outside. Here L is the height of the foam along the x direction.

from Eq. (2):

$$\frac{\partial P}{\partial x} = \frac{1}{2}\beta\frac{\gamma}{R}\frac{1}{\phi^{3/2}}\frac{\partial \phi}{\partial x}. \tag{3}$$

B. Some aspects of transport in liquid foams

1. Foam permeability

Drainage is defined as the flow of liquid in a foam due to a pressure gradient. It occurs spontaneously in macroscopic foamy materials, leading to a heterogeneous liquid fraction distribution, accelerating foam aging, and destabilization [8,25]. The liquid flow rate inside the foam, due to the pressure gradient, can be calculated only if the permeability of the foam L_H, defined in Eq. (1), is established; L_H depends on the foam properties (mainly the liquid fraction and the bubble radius) but also on the hydrodynamic boundary condition at the liquid-gas interface.

The model in [26] assumes that the flow only occurs in the Plateau borders and that the contribution of the films and nodes is negligible. In the rigid interface limit case, the permeability factor then reads

$$L_H = \frac{K}{\eta}R^2\phi^2, \tag{4}$$

where K is a geometrical factor calculated numerically ($K = 0.0032$).

An extension of this model [27] has been proposed, also taking into account the dissipation in the nodes. In the limit of mobile interfaces, the dissipation in the PBs becomes negligible and the permeability is given by

$$L_H = \frac{H}{\eta}R^2\phi^{3/2}, \tag{5}$$

with $H = 0.0023$ obtained numerically [18].

In practice, even for surfactants which are expected to create mobile interfaces, the foam permeability is larger than the one calculated by Eq. (5). As reported in the literature [10,18,28], experiments made with various surfactants and different bubble sizes have a permeability that scales as ϕ^n, with n varying between 1.5 and 2 as a function of the surface mechanical properties.

2. Foam conductance

When an oscillatory voltage difference is applied on the foam material, one can measure the current in the foam to deduce the foam conductivity G. It has been shown experimentally that it depends mainly on the bulk liquid conductivity σ and on the liquid fraction of the foam [29]. In the case of a large liquid fraction, the curve is well described by the Maxwell bubbly liquid limits [30], whereas at small liquid fraction, one can consider the foam as an array of PBs, evenly oriented, that transport the ions. This situation, described by Lemlich [31] and reasonable in the limit of dry foam (typically when $\phi < 3\%$), reads

$$G = \tfrac{1}{3}\sigma\phi. \tag{6}$$

3. Thermo-osmosis

The flows induced by a thermal gradient have been less studied in the literature. The exact origin of so-called thermo-osmosis is still debated and even the direction of the induced flows is difficult to predict [15,32,33]. In the case of liquid foams, some experiments have been carried out in two-dimensional foams (an assembly of bubbles squeezed between two plates) [13,19]. They show that a thermal gradient will induce a thermal Marangoni stress along the bubble interfaces and then induce a flow that can even reverse gravity-driven drainage. Different mechanisms taking into account an opposite generated interfacial stress due to inhomogeneous surfactant distribution are also relevant when surfactant properties are tuned [13].

4. Electro-osmosis

Since Reuss's experiments, generating a liquid flow with an electric field (or in the case of its phoresis counterpart, generating solid motion in liquids) has been extensively investigated in colloidal science [34]. The velocity of the liquid is set by the applied electric field and is given by the so-called Smoluchowski equation, namely,

$$v = -\frac{\epsilon\zeta}{\eta}E, \tag{7}$$

where ζ is the zeta potential of the interface, which characterizes its electrostatic and hydrodynamic environment [2]. A recent review [35] and some recent experiments [14] underline the difficulties of measuring accurately the ζ potential of an interface covered with ionic surfactants.

The effect of a vertical electric field on a macroscopic foam has been investigated experimentally [36–39] and has regained interest recently [40], especially at a more local scale, in the films and in the PBs [41–43]. However, a complete description of an electro-osmotic flow in such a deformable system is still lacking. Working towards a better description, we try to identify the factor α, which is defined in the Onsager matrix and which describes these coupled effects. With an assumption similar to the one performed in the Lemlich model of conductance (Sec. II B 2), we will consider that the electro-osmotic flow occurs only in the Plateau borders, evenly oriented, which results in

$$\alpha = -\frac{\phi}{3}\frac{\epsilon\zeta}{\eta}. \tag{8}$$

III. GENERAL RELATIONSHIPS

In the following, the case of a liquid foam, with a Kelvin structure, with bubbles of constant radius R and a liquid fraction ϕ typically smaller than 3%, is investigated. We will neglect the effect of gravity and assume that there is no thermal gradient. An electric potential difference ΔU is applied on either side of the foam, in the x direction, by two electrodes separated by a distance L and with an area $\mathcal{A}$ (Fig. 4).

We will define how the liquid fraction in the foam is affected by the applied electric field and plot the liquid fraction profile in several conditions. Throughout the paper, we will assume that the

zeta potential of the interface is negative, hence that the electro-osmotic flow will occur in the same direction as the electric field (towards increasing x here).

A. Liquid fraction profile

We can relate the flow rate of liquid Q and ionic current I to the pressure gradient ∇P and the applied electric field $-\nabla U$ by local linear response (where U is the electric potential) [see Eq. (1)]:

$$Q = -\mathcal{A}\left(L_H \frac{\partial P}{\partial x} + \alpha \frac{\partial U}{\partial x}\right), \quad I = -\mathcal{A}\left(\alpha \frac{\partial P}{\partial x} + G \frac{\partial U}{\partial x}\right). \tag{9}$$

The different parameters such as the hydrodynamic permeability L_H, the ionic conductance in the foam G, and the coupled term α depend only on the liquid fraction ϕ (and then indirectly of x and t). These equations can be completed by mass conservation

$$\mathcal{A}\frac{\partial \phi}{\partial t}(x,t) = -\frac{\partial Q}{\partial x}(x,t) \tag{10}$$

and the electric charge conservation. In contrast to mass, variations of the electric charge over time are instantaneous, so the electrical current is conserved at every moment.

$$\frac{\partial I}{\partial x}(x,t) = 0. \tag{11}$$

Then the current does not depend on x and is denoted by $I(t)$. We finally assume that the foam structure, and subsequently its liquid fraction, instantaneously adapts to the pressure. Under these assumptions, an equation for the temporal evolution of ϕ is derived from Eqs. (9) and (10):

$$\frac{\partial \phi}{\partial t}(x,t) = \frac{\partial}{\partial x}\left[\frac{\partial P}{\partial x}\left(L_H - \frac{\alpha^2}{G}\right) - \frac{I(t)}{\mathcal{A}}\frac{\partial}{\partial x}\frac{\alpha}{G}\right]. \tag{12}$$

The ratio α/G does not depend on the liquid fraction and then does not vary along the foam sample. The liquid fraction profile in the sample then satisfies

$$\frac{\partial \phi}{\partial t}(x,t) = \frac{\partial}{\partial x}\left[\frac{\partial P}{\partial x}\left(L_H - \frac{\alpha^2}{G}\right)\right]. \tag{13}$$

B. Boundary conditions

This equation is completed with boundary conditions depending on the geometry considered. We will present results for the two cases represented in Fig. 4.

1. Case A

In case A, the bottom of the foam is in contact with a reservoir whereas its top is in contact with an impermeable electrode. Then, at the bottom of the column ($x = 0$), the pressure is constant, which means for a dry foam that the liquid fraction is constant, defined as

$$\phi(0,t) = \phi_r. \tag{14}$$

A second boundary condition concerns the upper configuration: We assume that there is no flux at the impermeable electrode ($Q = 0$). This results in, from Eq. (9) applied for $x = L$,

$$L_H \frac{\partial P}{\partial x}\bigg|_{x=L} + \alpha \frac{\partial U}{\partial x}\bigg|_{x=L} = 0, \tag{15}$$

with $\frac{\partial U}{\partial x}|_{x=L}$ the voltage gradient at the electrode given by Eq. (9):

$$\left.\frac{\partial U}{\partial x}\right|_{x=L} = -\frac{I(t)}{\mathcal{A}G} - \left.\frac{\alpha}{G}\frac{\partial P}{\partial x}\right|_{x=L}. \tag{16}$$

The ionic current $I(t)$ is derived from the integration of this equation between 0 and L as the current does not depend on the spatial coordinate [see Eq. (11)]:

$$\Delta U = -\frac{I(t)}{\mathcal{A}}\int_0^L \frac{dx}{G} - \int_0^L \frac{\alpha}{G}\frac{\partial P}{\partial x}dx. \tag{17}$$

From this, the value of the current can then be expressed as a function of ϕ and replaced in Eq. (16) to determine the voltage gradient as a function of ϕ. Then the second boundary condition can be expressed with ϕ as the unique variable from a derivation of Eqs. (15)–(17). Note that in a steady state, this condition is simplified. Indeed, the flux is zero everywhere, so Eq. (15) can be directly integrated over the entire sample, resulting in

$$\Delta U = -\int_0^L \frac{L_H}{\alpha}\frac{\partial P}{\partial x}dx. \tag{18}$$

2. Case B

In the second case, the foam sample is squeezed between two electrodes and isolated from the outside. The first boundary condition is then volume conservation, which reads

$$\frac{1}{L}\int_0^L \phi(x,t)dx = \phi_i, \tag{19}$$

with ϕ_i the initial volume fraction. The second boundary condition of zero flux at the top and at the bottom of the sample, given by Eqs. (15)–(17), is in this case valid for $x = 0$ and $x = L$.

C. A few orders of magnitude

We assume that the initial liquid fraction profile is flat with a liquid fraction denoted by ϕ_i. To evaluate physically the different contributions governing liquid transport in our foam, we will consider a *typical* water-based liquid foam ($\eta = 10^{-3}$ Pa s) with a bubble radius $R = 100$ μm, a liquid fraction $\phi_i = 0.1\%$, a zeta potential of the surfactant-laden liquid-gas interface $\zeta = -100$ mV, a surface tension $\gamma = 34$ mN/m, and a conductivity of the soapy solution $\sigma = 600$ μS/cm. These parameters correspond to a liquid foam stabilized with sodium dodecyl sulfate near the critical micellar concentration. The size of the foam sample is set to $L = 5$ cm. We will now present some solutions of Eq. (13) in the two limits of rigid and mobile interfaces and for the different geometries, cases A and B, represented in Fig. 4.

IV. CASE OF RIGID INTERFACES

A. Liquid fraction equation

Using the definitions of L_H [Eq. (4)], α [Eq. (8)], G [Eq. (6)], and pressure gradient [Eq. (3)] previously introduced, the liquid fraction profile [Eq. (13)] satisfies

$$\frac{\partial \phi}{\partial t}(x,t) = \frac{\partial}{\partial x}\left[\frac{\gamma\beta}{2R}\frac{\partial \phi}{\partial x}\frac{1}{\sqrt{\phi}}\left(\frac{K}{\eta}R^2\phi - \frac{\epsilon^2\zeta^2}{3\eta^2\sigma}\right)\right]. \tag{20}$$

We introduce the following dimensionless variables: $X = x/L$ with L the vertical dimension of the foam sample, $\bar{\phi} = \phi/\phi_i$, and $T = t/\tau_r$ with τ_r a characteristic time (the timescale of the flow in the

foam due to capillary suction) defined as

$$\tau_r = \frac{2L^2\eta}{\gamma\beta RK\sqrt{\phi_i}}. \tag{21}$$

For our typical foam, τ_r is equal to 8500 s. This large value justifies our hypotheses that the liquid foam locally and instantaneously adjusts to the pressure. Moreover, a dimensionless number S_r, which compares the magnitude of coupled transport (electro-osmosis and streaming current) to the magnitude of direct transport (permeability), can be introduced. This parameter reads

$$S_r = \frac{\epsilon^2\zeta^2}{3\eta\sigma R^2 K\phi_i}. \tag{22}$$

The variations of the dimensionless liquid fraction then satisfies the relation

$$\frac{\partial\bar{\phi}}{\partial T} = \frac{\partial}{\partial X}\left(\frac{\partial\bar{\phi}}{\partial X}\frac{1}{\sqrt{\bar{\phi}}}(\bar{\phi} - S_r)\right). \tag{23}$$

The value of S_r is around 10^{-3} in our typical foam, which is small compared to one. In the following, we will then neglect the second term of Eq. (23). However, one must be careful when dry foams with small bubbles are considered ($S_r \simeq 1$ for a bubble size of $R = 10\ \mu$m). However, such out-of-equilibrium dry foams are coarsening and then the bubble size is increasing fast with time (on a timescale short compared to τ_r), resulting in a small and then negligible S_r. Equation (23) then reduces to

$$\frac{\partial\bar{\phi}}{\partial T} \simeq \frac{\partial}{\partial X}\left(\frac{\partial\bar{\phi}}{\partial X}\sqrt{\bar{\phi}}\right). \tag{24}$$

This equation, a diffusionlike equation with a small nonlinearity, is similar to the one of pressure-driven drainage. This means that coupled transport will affect the liquid fraction profile through the boundary conditions only. We begin by discussing the liquid fraction profiles in the steady state before studying the transient regime.

B. Some solutions of steady-state profile in specific conditions

In the steady-state case, Eq. (24) reduces to

$$0 = \frac{\partial}{\partial X}\left(\frac{\partial\bar{\phi}}{\partial X}\sqrt{\bar{\phi}}\right). \tag{25}$$

After an integration and the introduction of two constants $\bar{\phi}(0)$ and $\bar{\phi}(1)$, the liquid fraction at the bottom and at the top of the column, respectively, one recovers

$$\bar{\phi}(X) = \{\bar{\phi}(0)^{3/2} + [\bar{\phi}(1)^{3/2} - \bar{\phi}(0)^{3/2}]X\}^{2/3}. \tag{26}$$

To determine the values of $\bar{\phi}(0)$ and $\bar{\phi}(1)$, we consider the two cases A and B defined in Fig. 4.

1. Liquid fraction profile in case A: A foam in contact with a reservoir

In our dimensionless system, the first boundary condition is derived from Eq. (14),

$$\bar{\phi}(0) = \phi_r/\phi_i = \bar{\phi}_r. \tag{27}$$

The second is derived from Eq. (18) [with Eq. (3) to make explicit the pressure gradient] and is given by

$$[\sqrt{\bar{\phi}(1)} - \sqrt{\bar{\phi}(0)}] = \mathrm{Ca}_r, \tag{28}$$

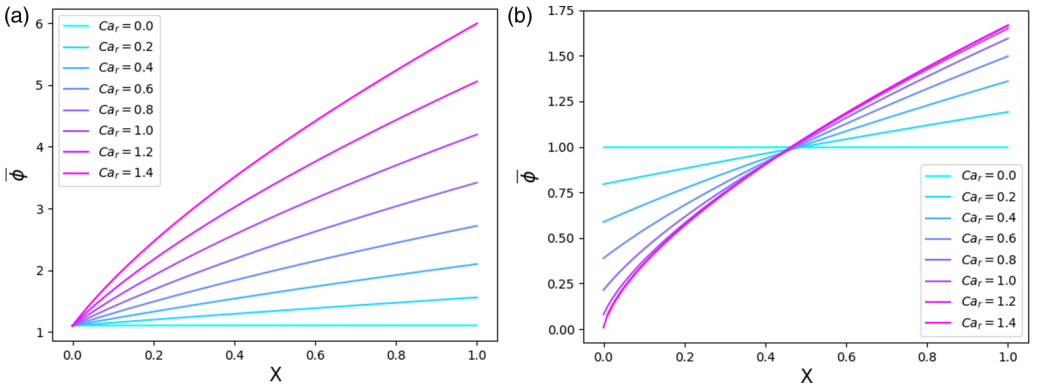

FIG. 5. Stationary liquid fraction profile for rigid interfaces in (a) case A from Eq. (30) with $\bar{\phi}_r = 1.1$ and (b) case B from Eq. (32).

with Ca_r an electro-osmotic capillary number, defined here in the rigid case, which compares the viscous stress generated by the electro-osmotic flow with the capillary pressure,

$$\mathrm{Ca}_r = -\frac{\epsilon\zeta\,\Delta U}{3\gamma R\beta K\sqrt{\phi_i}}. \tag{29}$$

We note that the zeta potential considered in this study is negative, resulting in a positive capillary number. For the typical foam considered here, with a voltage difference of 25 V, this capillary number is close to unity. Then the stationary liquid fraction profile in case A reads

$$\bar{\phi}(X) = \left\{\bar{\phi}_r^{3/2} + \left[(\mathrm{Ca}_r + \sqrt{\bar{\phi}_r})^3 - \bar{\phi}_r^{3/2}\right]X\right\}^{2/3}. \tag{30}$$

Liquid fraction profiles for different capillary numbers are reported in Fig. 5(a). One can observe that the total liquid fraction is increasing with the applied electric field or the capillary number. Electro-osmosis is then a useful tool to keep a foam wet. In particular, the liquid fraction at the top of the foam is very sensitive to the capillary number as it scales as Ca_r^2.

2. Liquid fraction profile in case B: An isolated foam

In this case, only the first boundary condition is modified and volume conservation is written

$$\int_0^1 \bar{\phi}(X)dX = 1. \tag{31}$$

The liquid fraction profile is derived from Eqs. (26), (30), and (31) and is given by

$$\bar{\phi}(X) = \tfrac{1}{4}\Big[\Big(-\mathrm{Ca}_r + \sqrt{2 - \mathrm{Ca}_r^2 + 2\sqrt{1 - \tfrac{2}{3}\mathrm{Ca}_r^2 + \tfrac{1}{5}\mathrm{Ca}_r^4}}\Big)^3 + 4\mathrm{Ca}_r\Big(3 - \mathrm{Ca}_r^2 + 3\sqrt{1 - \tfrac{2}{3}\mathrm{Ca}_r^2 + \tfrac{1}{5}\mathrm{Ca}_r^4}\Big)X\Big]^{2/3}. \tag{32}$$

This solution is plotted in Fig. 5(b) for different capillary numbers. From a constant liquid fraction without an electric field, one can see that some liquid is pumped from the bottom of the foam column to the top. One can also observe that if the capillary number is too large, the liquid fraction at the bottom of the column is vanishing, which is nonphysical: In this regime, the parameter S_r neglected so far becomes relevant. Moreover, one can notice that for large capillary numbers, the profile is converging. This can be explained by the fact that when the liquid fraction is locally too low, the capillary stress diverges and cannot be overcome.

C. Transient profile

In the transient state, we need to solve Eq. (24) with the boundary conditions defined previously (Sec. III B).

1. Boundary conditions

The boundary conditions of constant liquid fraction at the bottom of the column [case A, Eq. (14)] and of volume conservation in the sample [case B, Eq. (31)] remain valid when an unsteady state is described. In contrast, as mentioned in Sec. III B 1, the boundary condition of nonflux at the electrode is now given by Eqs. (15)–(17). To get these boundary conditions dimensionless, we introduce the dimensionless current $\bar{i}(t) = I(t)/I_i$ with

$$I_i = \frac{1}{3}\frac{\Delta U \sigma \phi_i \mathcal{A}}{L}, \tag{33}$$

which corresponds to the initial current under the applied voltage ΔU. Then Eq. (16) reads

$$\frac{\partial \bar{U}}{\partial X} = -\frac{\bar{i}(T)}{\bar{\phi}} - \frac{S_r}{2\,\mathrm{Ca}_r}\frac{1}{\bar{\phi}^{3/2}}\frac{\partial \bar{\phi}}{\partial X}. \tag{34}$$

If once again we consider that $S_r \ll 1$ or even $S_r \ll \mathrm{Ca}_r$, the electrical current at each time reduces to

$$\bar{i}(T) = \frac{1}{\int_0^1 \frac{1}{\bar{\phi}(\bar{X},T)} dX}, \tag{35}$$

and together with the boundary condition [no flux at the electrode (15)], one recovers

$$2\,\mathrm{Ca}_r \bar{i}(T) = \sqrt{\bar{\phi}(1)}\left.\frac{\partial \bar{\phi}}{\partial X}\right|_{X=1}. \tag{36}$$

Note that in this transient case, $\bar{\phi}(1)$ and its spatial derivatives are a function of time T. We will first consider the limit case of a liquid fraction distribution that remains close to the initial one and then make a full numerical resolution of these equations.

2. Small applied electric field: Linear regime

We first consider the case of small applied voltage, namely, $\mathrm{Ca}_r \ll 1$. In this limit, the liquid fraction is given by $\bar{\phi} = 1 + \epsilon$ with $\epsilon \ll 1$. The equations describing the liquid fraction evolution (24) and the boundary conditions are then linearized. The variation of ϵ versus space and time satisfies the classical diffusion equation

$$\frac{\partial \epsilon}{\partial T} \simeq \frac{\partial}{\partial X}\left(\frac{\partial \epsilon}{\partial X}\right). \tag{37}$$

The boundary conditions are now inspected under this hypothesis for cases A and B.

a. Case A. The contact with the liquid tank sets the liquid fraction at the bottom of the column $\epsilon(0, T) = \bar{\phi}_r - 1$. The second boundary condition [given by Eqs. (35) and (36)] can be also linearized and results in $\partial\epsilon/\partial X|_{X=1} \simeq 2\mathrm{Ca}_r$. This condition on the flux of the diffusive quantity ϵ shows that electro-osmosis fixes a pressurelike condition on the system.

Then the solution is given by

$$\epsilon(X, T) = \mathcal{L}^{-1}(\hat{\epsilon}(p, X)), \tag{38}$$

with $\hat{\epsilon}(p, X)$, the Laplace transform of $\epsilon(X, t)$, given by

$$\hat{\epsilon}(p, X) = \frac{\phi_r - 1}{p}\cosh(qX) + \frac{2\mathrm{Ca}_r - q(\phi_r - 1)\sinh(q)}{pq\cosh(q)}\sinh(qX), \tag{39}$$

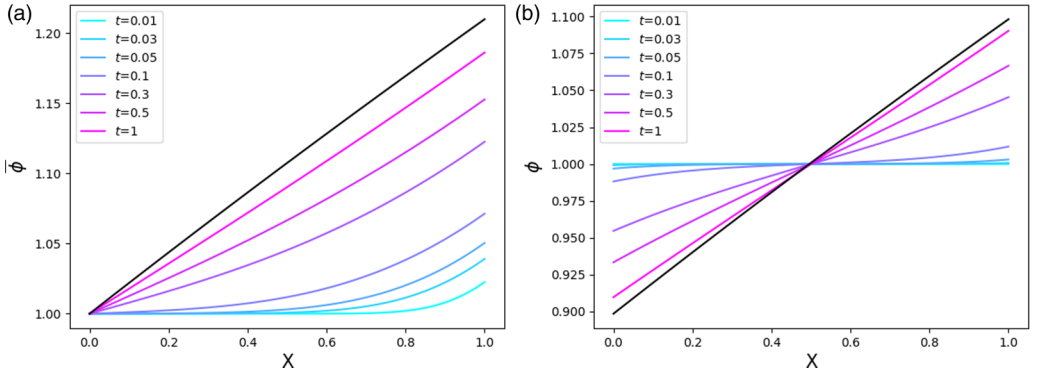

FIG. 6. Linearized transient liquid fraction profile for rigid interfaces plotted at different times T with $\mathrm{Ca}_r = 0.1$ in (a) case A (with $\bar{\phi}_r = 1$) and (b) case B. The black line corresponds to the steady-state profile obtained from Eqs. (30) and (32) for cases A and B, respectively.

with $q^2 = p$. To evaluate the inverse Laplace transform, we use the invert Laplace transform function [44]. Some liquid fraction profiles plotted at different dimensionless times are reported in Fig. 6(a) for $\mathrm{Ca}_r = 0.1$ and $\bar{\phi}_r = 1$.

b. Case B. In this second case, the first condition is given by volume conservation, namely, $\int_0^1 \epsilon(X)dX = 0$. The system is then symmetrical with respect to $X = 1/2$ with $\epsilon(1/2) = 0$. The solution reads

$$\epsilon(x,t) = \mathcal{L}^{-1}(\hat{\epsilon}(p,x)), \tag{40}$$

with

$$\hat{\epsilon}(p,X) = \frac{2\,\mathrm{Ca}_r \sinh[q(X-1/2)]}{pq\cosh(q)}. \tag{41}$$

Let us note that in this case, ϵ is directly proportional to the capillary number. This function is represented in Fig. 6. Finally, in these two cases, the profile at short times adapts to the boundary (up to $T = 0.02$) and then slowly relaxes entirely towards a linear equilibrium.

3. Numerical solution

Equation (24) can also be solved numerically, using an explicit scheme, with the appropriate boundary conditions that apply in cases A and B. Liquid fraction profiles are plotted in Fig. 7, with $\mathrm{Ca}_r = 1$. We can observe that the diffusion mechanism (from the border) is similar to the linear case, but with a relaxation towards the nonlinear stationary profile.

V. CASE OF MOBILE INTERFACES

In this section we apply the same methodology to determine the profile of the liquid fraction in the case of mobile interfaces.

A. Liquid fraction equation

In this case the equation describing the temporal and spatial variations of the liquid fraction is derived from Eqs. (13) and (5):

$$\frac{\partial\phi}{\partial t}(x,t) = \frac{\partial}{\partial x}\left[\frac{\gamma\beta}{2R}\frac{\partial\phi}{\partial x}\frac{1}{\sqrt{\phi}}\left(\frac{H}{\eta}R^2\sqrt{\phi} - \frac{\epsilon^2\zeta^2}{3\eta^2\sigma}\right)\right]. \tag{42}$$

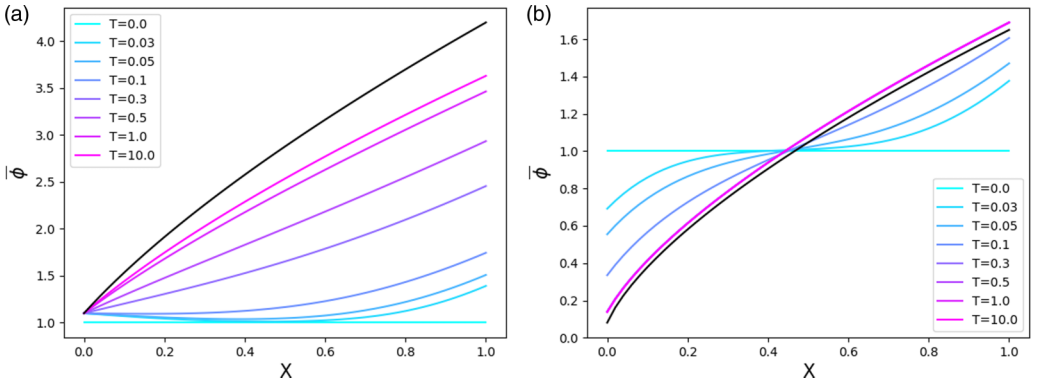

FIG. 7. Liquid fraction profile obtained numerically for rigid interfaces in (a) case A (with $\bar{\phi}_r = 1.1$) and (b) case B with $\mathrm{Ca}_r = 1$.

As for the rigid case, we introduce similar dimensionless variables $X = x/L$, $\bar{\phi} = \phi/\phi_i$, and $T = t/\tau_m$ with

$$\tau_m = \frac{2\eta L^2}{\gamma\beta H R} \tag{43}$$

and the dimensionless number $S_m = \frac{\epsilon^2\zeta^2}{3\eta\sigma H R^2\sqrt{\phi_i}}$. In the case of our typical foam, the characteristic time is 375 s (so one order of magnitude faster than in the rigid case) and $S_m = 4 \times 10^{-5}$, which is definitely small compared to one. In this case also we will neglect the coupling contribution. Then Eq. (46) simplifies directly in a linear diffusive equation

$$\frac{\partial\bar{\phi}}{\partial T} \simeq \frac{\partial^2\bar{\phi}}{\partial X^2}. \tag{44}$$

B. Some solutions of steady-state profile in specific conditions

The equation governing the liquid fraction distribution is given by

$$0 \simeq \frac{\partial^2\bar{\phi}}{\partial X^2}, \tag{45}$$

which can be easily integrated in

$$\bar{\phi}(X) = [\bar{\phi}(1) - \bar{\phi}(0)]X + \bar{\phi}(0), \tag{46}$$

introducing once again the liquid fraction at the bottom and at the top of the column $\bar{\phi}(0)$ and $\bar{\phi(1)}$, respectively.

1. Boundary conditions and solution in case A

We consider here the case A of a foam in contact with a liquid tank. The liquid fraction at the bottom of the foam is then given by $\bar{\phi}(0) = \bar{\phi}_r$.

Similarly to what has been performed in the case of rigid interfaces, current conservation and the no-flux condition at the top electrode reads

$$\frac{1}{\bar{\phi}(X)}\frac{\partial\bar{\phi}}{\partial X} = \mathrm{Ca}_m\frac{\partial\bar{U}}{\partial X}, \tag{47}$$

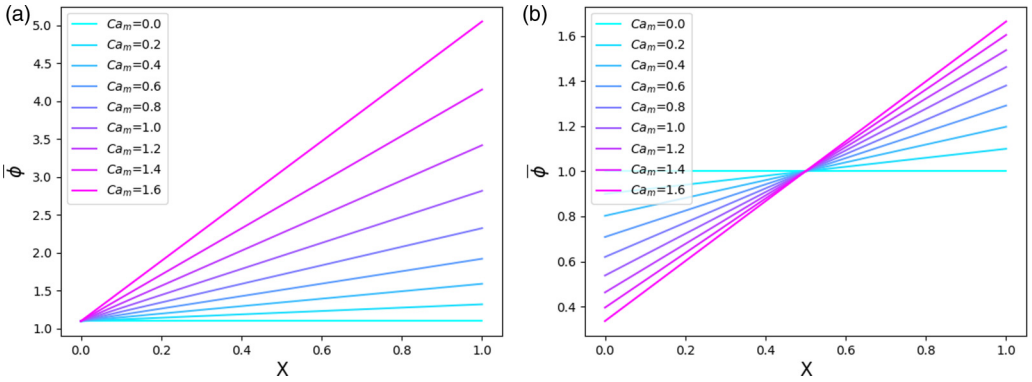

FIG. 8. Stationary liquid fraction profile for mobile interfaces in (a) case A (with $\bar{\phi}_r = 1.1$) and (b) case B.

with the electro-osmotic capillary number Ca_m defined as

$$\mathrm{Ca}_m = -\frac{\epsilon\zeta\,\Delta U}{\gamma L}\frac{2L}{3HR\beta}. \tag{48}$$

Note that, in contrast to the rigid case, Ca_m does not depend on the initial liquid fraction ϕ_i. For a difference of voltage of 25 V as before, with our typical foams, the order of magnitude of Ca_m is around 0.08, definitely smaller than Ca_r. After an integration over the entire sample (within X), the second condition is given by

$$\ln\left(\frac{\bar{\phi(1)}}{\bar{\phi(0)}}\right) = \mathrm{Ca}_m \tag{49}$$

and the liquid fraction profile by

$$\bar{\phi}(X) = \bar{\phi}_r[\exp(\mathrm{Ca}_m) - 1]X + \bar{\phi}_r. \tag{50}$$

This solution is represented in Fig. 8 for different capillary numbers. The liquid fraction at the top of the column is varying exponentially with the capillary number and then the applied electric field, allowing one to maintain liquid in the foam very efficiently. However, in this case, increasing Ca_m up to unity requires a huge applied voltage (around ∼500 V), which is difficult to reach practically.

2. Boundary conditions and solution: Case B

In the case of an isolated foam squeezed between two electrodes, the first boundary condition is given by volume conservation as before $\int_0^1 \bar{\phi}(X)dX = 1$ and the full solution then reads

$$\bar{\phi}(X) = 2\tanh\left(\frac{\mathrm{Ca}_m}{2}\right)X + \frac{2}{e^{\mathrm{Ca}_m}+1}. \tag{51}$$

The profile is also reported in Fig. 8 for different capillary numbers. A symmetric linear profile is recovered.

When the foam is squeezed between two electrodes, variations of the liquid fraction as a function of the position first increase greatly with Ca_m and then saturate at large capillary numbers, as observed for the rigid case, in the same geometry. Once again, the saturation is due to the fact that the capillary stress is nonlinear and increases when the foam dries, explaining why a saturation is not observed in case A, when the foam is in contact with a reservoir. Then, above a certain applied electric field, the capillary pressure is too large to be overcome in the dry zones and the liquid fraction profile does not evolve anymore.

C. Transient profile

We now attempt to define the transient liquid fraction profile when mobile interfaces are considered. Note that in contrast to rigid cases, Eq. (45) is a diffusion equation without any hypothesis on the Ca_m value. The normalized equation (45) is solved by taking into account the boundary conditions adapted to cases A and B. Similarly to Sec. IV C 1, one can show that the electric current is linked to the voltage gradient according to

$$\frac{\partial \bar{U}}{\partial X} \simeq \frac{i(T)}{\bar{\phi}}, \tag{52}$$

with

$$i(T) = \frac{1}{\int_0^1 \frac{1}{\phi(\bar{X},T)} dX}, \tag{53}$$

and then the no-flux condition reads

$$i(T) = \frac{1}{\mathrm{Ca}_m} \frac{\partial \bar{\phi}}{\partial X}\bigg|_{X=1}, \tag{54}$$

so the problem is closed in both cases.

1. Small applied electric field: Linear regime

For small capillary numbers, if once again we define the liquid fraction as $\bar{\phi}(X) \simeq 1 + \epsilon(X)$ with $\epsilon(X) \ll 1$, one recovers, in $X = 1$,

$$\frac{\partial \epsilon}{\partial X}\bigg|_{X=1} = \mathrm{Ca}_m. \tag{55}$$

So, as before, one can recover the liquid fraction profile in the two cases considered here.

a. Case A. In this first case, the second condition reads as usual $\epsilon(0) = \phi_r - 1$. Then the solution is given by

$$\epsilon(x,t) = \mathcal{L}^{-1}(\hat{\epsilon}(p,x)), \tag{56}$$

with

$$\hat{\epsilon}(p,X) = \frac{\phi_r - 1}{p}\cosh(qX) + \frac{\mathrm{Ca}_m - q(\phi_r - 1)\sinh(q)}{pq\cosh(q)}\sinh(qX). \tag{57}$$

This solution is represented in Fig. 9, as performed for the rigid case.

b. Case B. In this second case, the second boundary condition is given by volume conservation, namely, $\int_0^1 \epsilon(X)dX = 0$. The system is then symmetrical with respect to $X = 1/2$ where $\epsilon(1/2) = 0$. The solution then reads

$$\epsilon(x,t) = \mathcal{L}^{-1}(\hat{\epsilon}(p,x)), \tag{58}$$

with

$$\hat{\epsilon}(p,X) = \frac{\mathrm{Ca}_m \sinh[q(X-1/2)]}{pq\cosh(q)}. \tag{59}$$

This function is represented in Fig. 9.

2. Numerical solution

The equations are also solved using an explicit scheme and results are reported in Fig. 10. Once again, a diffusion process emerging from the borders accompanies a relaxation to the linear steady-sate profile.

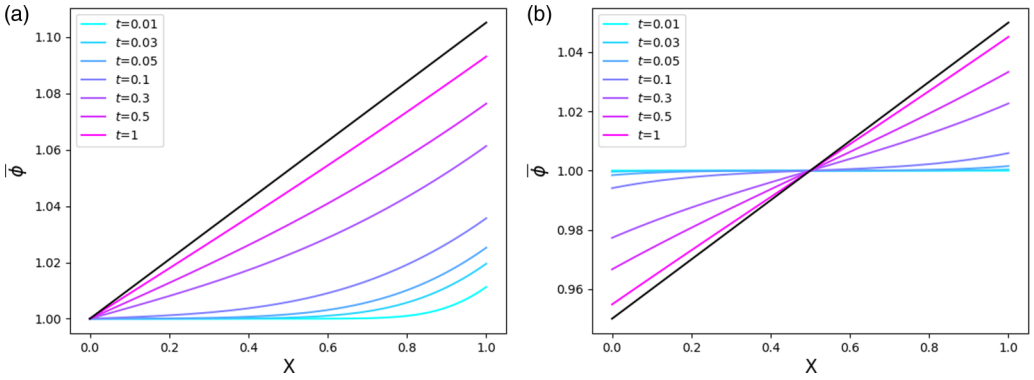

FIG. 9. Linearized liquid fraction profile as a function of the position for different times T for (a) case A and (b) case B. We set $\mathrm{Ca}_m = 0.1$ and $\bar{\phi}_r = 1$ to remain in the linear regime.

VI. DISCUSSION

We now compare the results obtained in different cases (a foam in contact with a reservoir or a foam squeezed between two electrodes) and in different regimes (mobile and rigid interfaces). We will then discuss the different hypotheses made during the previous calculation.

A. Comparison of different cases

The evolution of the liquid fraction profile of a liquid foam subjected to an electric field was determined using several hypotheses. Unexpectedly, the general equation that describes the liquid distribution within the foam does not depend on the applied electric field and is diffusivelike (with a small nonlinearity in the rigid case). As for classical mass transport in a foam under a pressure gradient, two characteristic times depending on the interface rigidity, defined as τ_r and τ_m, can be introduced and differ by several orders of magnitude.

The effect of the electric field is introduced through the boundary conditions and will affect dramatically the final steady-state profile. Its magnitude can be evaluated by introducing an electro-osmotic capillary number that compares the viscous stress associated with the electro-osmotic flow and the capillary pressure.

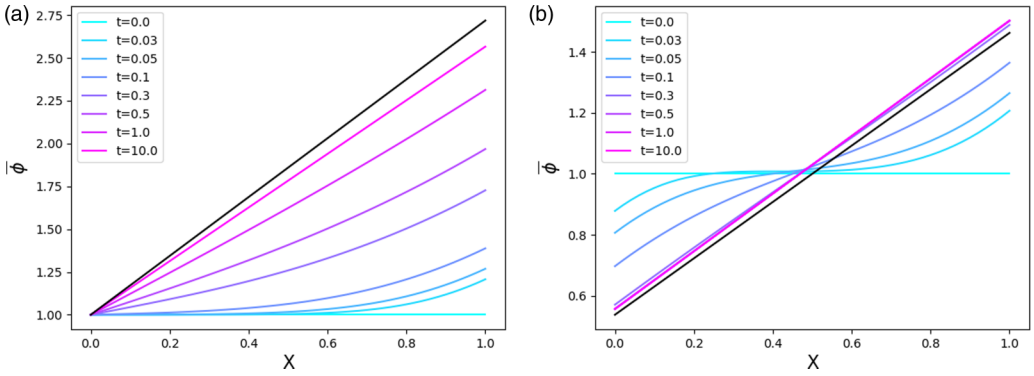

FIG. 10. Numerical solutions obtained in (a) case A and (b) case B for liquid fraction evolution, at different times with $\mathrm{Ca}_m = 1$ and $\phi_r = 1.1$. The black lines correspond to the stationary profiles determined from Eq. (50) for case A and Eq. (51) for case B.

In the first geometry considered (case A), the foam can capture water from the reservoir. However, the case of a reservoir filled with liquid is not realistic as the foam liquid fraction at the top is expected to be larger than the random close packing liquid fraction (imposed at the bottom in this case). It is then not a foam anymore but a bubbly liquid and the equations established are no longer valid. The analysis developed here describes situations of a foam, for example, in contact with a water-based gel and which captures liquid under an applied electric field.

One can also compare the pumping efficiency of a foam squeezed between two electrodes (case B) in the steady-state regime for the two limits of rigid and mobile interfaces. For our typical foam and for an applied electric field of 25 V, in the case of rigid interfaces, the difference of liquid fraction ratio between the top and the bottom of the foam is equal to 1.6, whereas in the case of mobile ones, it is equal to 0.08. The rigid foam is then more efficient, despite the long timescales required to achieve equilibrium. The different hypotheses performed (no gravity, extreme cases of rigid and mobile interfaces, dry foams, large bubbles, and no contribution of the films in the transport) will be discussed in the following section.

B. Discussion of the hypotheses

1. Effect of liquid fraction

The analysis has been performed in the case of dry foams, a hypothesis that should be kept during the entire process. If the foam liquid fraction is increased, the description of L_H, α, and G will differ. Some other difficult aspects concern the definition of the pressure. In particular, when we consider the geometry A of a liquid in contact with a reservoir, the condition is a fixed so-called osmotic pressure at the bottom of the column, which can differ from the capillary pressure and whose expression is detailed in [23].

2. Contribution of the films

In this analysis we neglected the contribution of the films in the transport, similarly to what is generally performed for pressure-driven drainage. However, this hypothesis can be discussed. For drainage, the film contribution was mentioned because film thicknesses were observed to be high [28]. A recent work has shown that during electro-osmosis in a single soap film, a thickening of the film was observed [35,41]. The thickness of the film δ is determined by a balance between the electro-osmotic flow and the capillary suction. It is given by, introducing Ca_f, an electro-osmotic capillary number based on film geometry

$$\delta = 2.68r\left(\frac{\epsilon_0\epsilon_r|\zeta|\Delta U}{\gamma L}\right)^{2/3} = 2.68r\,\mathrm{Ca}_f^{2/3}, \tag{60}$$

where r is the equivalent of the radius of curvature of the Plateau border.

If we consider our typical foam and if we apply a voltage of 20 V, the film thickness predicted by this expression is 0.2 nm, much smaller than the thickness of a film at equilibrium. Thus, this process does not affect the film thickness in this limit. If we consider a wetter foam ($\phi = 5\%$ with a bubble radius of 2 mm), the film thickness can reach 20 nm, a value still quite low. However, the contribution of the film on transport properties will be significant for very dry foams and will be larger than the one in the Plateau borders if $\phi \leqslant \mathrm{Ca}_f^{4/3}$. This corresponds to a liquid fraction below 0.001%.

As a first-order correction, the effect of film thickening can be neglected in the hydrodynamic permeability L_H whether the rigid or mobile case is considered (for rigid films, for example, the permeability in one film is proportional to δ^3, so even if the film thickens, it remains negligible as compared to the contribution of the Plateau borders). In contrast, if we consider other types of transport, where plug profiles are expected (for the conductance G or for the electro-osmotic coupling α), the contribution of the films to the total transport will be proportional to ratio of the liquid volume in the film to the total liquid volume and is generally significant. One interesting point

is that intrinsically, as the mechanisms of transport are of same nature (plug flows), the ratio α/G is always independent of the liquid fraction and then independent of the spatial position x. This characteristic is a specific to liquid foams.

3. Effect of gravity

The effect of gravity is considered by adding the gravitational external force in the system. This term can be incorporated, for example, in the pressure. The equations that fix the liquid fraction for the rigid [Eq. (20)] and mobile [Eq. (46)] cases are modified to become classical gravity drainage equations [10], introducing a Bond number which reads $\mathrm{Bo} = 2\rho g L R\sqrt{\phi_i}/\gamma\beta$. The problem however differs from classical drainage because of the boundary conditions. A promising avenue would be to solve the problem in the presence of gravity and to determine the electric field required to reverse gravity-driven drainage.

4. Effect of surface viscoelasticity

In the stationary state, surface properties will affect the permeability of the foam but not the conductance or the electro-osmotic contribution. Therefore, the consequences of adding surface viscoelasticity will be similar to the ones for gravity-driven drainage [10], ranging between the two limit cases (rigid and mobile interfaces) described here.

In transient regimes or when an oscillating field is applied, one has to consider surfactant ability to desorb, resorb, and create Marangoni stresses along the interface. One has to compare the different timescales involved in surfactant dynamics, which depend on surfactant type (adsorption-desorption time and diffusion time at the interface or in the bulk), and the period of actuation.

5. Effect of bubble size

The bubble size affects different factors in this complex problem. It is first encountered in the definition of the capillary number, which does not depend on the total electric field but on the total voltage difference applied on one bubble size. So the larger the bubbles, the smaller the capillary number for a given applied voltage. Moreover, the characteristic times of the transient regime increase when R is decreased. Then the larger the bubbles, the shorter the transient.

The last factor in which it is encountered is in the magnitude of coupled transport, through the parameter S defined in both cases. For foams with small bubbles around 10 μm, S is no longer negligible. Note that the bubble radius growth, due to coarsening, after a transient of 10 min, reaches a self-similar evolution [45]: The smaller the bubbles, the faster the relative radius evolution. Finally, foam polydispersity will affect the results here particularly through the R dependences in the different parameters introduced and thus must be taken into account.

C. Comparison with experimental data

A few experiments have been performed to show the effect of an electric field on flow in liquid foam [35,36,38–40]. Due to the lack of information on experimental details and foam properties, a comparison can be achieved only in one case [35]. We thus report in Table I the ratio of the volume of liquid observed in the sample in the presence of the electric field $\Omega(\mathrm{Ca})$ divided by the initial volume Ω and the electro-osmotic capillary number Ca deduced from the experiments. To compare with our predictions, we calculate the excess of liquid in the foam (situation A) as

$$\frac{\Omega(\mathrm{Ca})}{\Omega} = \frac{\int_0^L \phi(x,\mathrm{Ca})dx}{\int_0^L \phi(x,0)dx}, \tag{61}$$

with $\phi(x)$ given by Eq. (30) as the surfactant employed (sodium dodecyl sulfate) can be considered as generating rigid interfaces. A clear comparison is difficult as these experiments are performed under gravity, with one electrode set in the liquid. The value of ϕ_r is then difficult to determine and is taken at $\bar{\phi}_r = 0.1$ arbitrarily. A full comparison would require an analysis which takes these

TABLE I. Comparison between experimentally observed normalized volume electro-osmotic liquid retention (Expt.) [35] and theoretical expectations from Eq. (61) (Theor.). The case considered is case A with rigid interfaces. The foam initial liquid fraction is $\phi_i = 0.005$, the bubble radius is $R = 3$ mm, the solution surface tension is $\gamma = 34$ mN/m, and $\bar{\phi}_r$ has been set arbitrarily to 0.1. Note that the ratio both experimentally and theoretically is taken with a reference not at $\mathrm{Ca}_r = 0$ but at $\mathrm{Ca}_r = 0.01$.

$(\Omega(\mathrm{Ca})/\Omega)_{\mathrm{Expt.}}$	Ca_r	$(\Omega(\mathrm{Ca})/\Omega)_{\mathrm{Theor.}}$
1.15	0.05	1.14
1.25	0.1	1.33
1.3	0.14	1.5

factors into account. Indeed, despite linear response theory, the gravity-driven drainage is not only superimposed over electro-osmosis, as it will affect also the foam structure (i.e., liquid fraction) and then the transport coefficient of the Onsager matrix. Experiments varying the liquid fraction and bubble size, together with theoretical development taking into account gravity, are thus required to fully describe these phenomena.

VII. CONCLUSION AND FUTURE DIRECTIONS

We have predicted the spatial distribution of liquid in a foam in the presence of an applied electric field, which induces electro-osmosis in the foam structure. This analysis is performed in two particular regimes: the case of surfactants that generate a no-slip boundary condition for the liquid velocity at liquid gas interfaces (so-called rigid interfaces) and the case of surfactants that generate stress-free boundary conditions (so-called mobile interfaces). In both cases we have shown that the equation describing the liquid fraction profile evolution does not depend on the applied electric field and is diffusivelike. Both tendencies are similar (except for a small nonlinearity for the rigid case) but timescales involved can vary by several orders of magnitude. The influence of the electric field appears in the boundary conditions, which will of course dramatically affect the profile. We introduced a dimensionless number that compares the magnitude of the viscous stress generated by the electro-osmotic flow and the capillary pressure in the complex foam geometry, designated the capillary electro-osmotic number (Ca_r or Ca_m).

This analysis is an initial attempt towards the understanding of such a system. Apart from obvious improvements, such as introducing gravity or interfacial viscoelasticity, one must note that a realistic description would be much more complex. Indeed, a foam is an out-of-equilibrium medium that evolves with time, due, for example, to coarsening, coalescence, or evaporation. All these mechanisms will affect and will be affected by the foam structure and dynamics. To give just one example of these intricate couplings, coarsening, on the one hand, will affect the bubble size versus time and then the magnitude of the electro-osmotic flow in the foam. On the other hand, the coarsening depends on the local liquid fraction and on the film thickness and is affected by the magnitude of the electro-osmotic flow. Such effects then have to be fully incorporated for a complete description of foam evolution under an electric field. On a more practical side, experiments must be performed to determine whether electro-osmosis can indeed be useful to retain liquid in a foam sample and then increase foam homogeneity and stability [46] over time.

ACKNOWLEDGMENTS

We would like to thank C. Ybert, F. Detcheverry, L. Joly, B. Blanc, and M. Le Merrer for enlightening discussions and L. O'Connell for a critical reading of the manuscript.

[1] F. F. Reuss, Mem. Soc. Imp. Nat. Moscou **2**, 327 (1809).
[2] L. Bocquet and E. Charlaix, Nanofluidics, from bulk to interfaces, Chem. Soc. Rev. **39**, 1073 (2010).
[3] G. A. H. Elton, Electroviscosity. I. The flow of liquids between surfaces in close proximity, Proc. R. Soc. London Ser. A **194**, 259 (1948).
[4] G. A. H. Elton, Electroviscosity. II. Experimental demonstration of the electroviscous effect, Proc. R. Soc. London Ser. A **194**, 275 (1948).
[5] G. A. H. Elton, Electroviscosity III. Sedimentation phenomena in ionic liquids, Proc. R. Soc. London Ser. A **197**, 568 (1949).
[6] L. Bocquet and P. Tabeling, Physics and technological aspects of nanofluidics, Lab Chip **14**, 3143 (2014).
[7] L. Onsager, Reciprocal relations in irreversible processes. I., Phys. Rev. **37**, 405 (1931).
[8] I. Cantat, S. Cohen-Addad, F. Elias, F. Graner, R. Höhler, O. Pitois, F. Rouyer, and A. Saint-Jalmes, *Foams: Structure and Dynamics* (Oxford University Press, Oxford, 2013).
[9] D. Weaire and R. Phelan, A counter-example to Kelvin's conjecture on minimal surfaces, Philos. Mag. Lett. **69**, 107 (1994).
[10] S. Cohen-Addad, R. Höhler, and O. Pitois, Flow in foams and flowing foams, Annu. Rev. Fluid Mech. **45**, 241 (2013).
[11] N. V. Churaev, J. Ralston, I. P. Sergeeva, and V. D. Sobolev, Electrokinetic properties of methylated quartz capillaries, Adv. Colloid Interface Sci. **96**, 265 (2002).
[12] L. Joly, C. Ybert, E. Trizac, and L. Bocquet, Hydrodynamics Within the Electric Double Layer on Slipping Surfaces, Phys. Rev. Lett. **93**, 257805 (2004).
[13] V. Miralles, E. Rio, I. Cantat, and M.-C. Jullien, Investigating the role of a poorly soluble surfactant in a thermally driven 2D microfoam, Soft Matter **12**, 7056 (2016).
[14] B. Blanc, O. Bonhomme, P.-F. Brevet, E. Benichou, C. Ybert, and A.-L. Biance, Electroosmosis near surfactant laden liquid-air interfaces, Soft matter **14**, 2604 (2018).
[15] L. Fu, S. Merabia, and L. Joly, What Controls Thermo-Osmosis? Molecular Simulations Show the Critical Role of Interfacial Hydrodynamics, Phys. Rev. Lett. **119**, 214501 (2017).
[16] C. Navier, Mémoire sur les lois du mouvement des fluides, Mem. Acad. R. Sci. Inst. France **6**, 389 (1823).
[17] L. Joly, F. Detcheverry, and A.-L. Biance, Anomalous ζ Potential in Foam Films, Phys. Rev. Lett. **113**, 088301 (2014).
[18] M. Durand, Contributions théorique et expérimentale à l'étude du drainage d'une mousse aqueuse, Ph.D. thesis, Université Paris Sud–Paris XI, 2002.
[19] V. Miralles, B. Selva, I. Cantat, and M.-C. Jullien, Foam Drainage Control Using Thermocapillary Stress in a Two-Dimensional Microchamber, Phys. Rev. Lett. **112**, 238302 (2014).
[20] P. Huang and K. S. Breuer, Direct measurement of slip length in electrolyte solutions, Phys. Fluids **19**, 028104 (2007).
[21] D. M. Huang, C. Cottin-Bizonne, C. Ybert, and L. Bocquet, Aqueous electrolytes near hydrophobic surfaces: Dynamic effects of ion specificity and hydrodynamic slip, Langmuir **24**, 1442 (2008).
[22] S. A. Koehler, S. Hilgenfeldt, E. R. Weeks, and H. A. Stone, Drainage of single plateau borders: Direct observation of rigid and mobile interfaces, Phys. Rev. E **66**, 040601 (2002).
[23] R. Höhler, Y. Y. C. Sang, E. Lorenceau, and S. Cohen-Addad, Osmotic pressure and structures of monodisperse ordered foam, Langmuir **24**, 418 (2008).
[24] A. Maestro, W. Drenckhan, E. Rio, and R. Höhler, Liquid dispersions under gravity: Volume fraction profile and osmotic pressure, Soft Matter **9**, 2531 (2013).
[25] E. Rio and A.-L. Biance, Thermodynamic and mechanical timescales involved in foam film rupture and liquid foam coalescence, Chem. Phys. Chem. **15**, 3692 (2014).
[26] G. Verbist, D. Weaire, and A. M. Kraynik, The foam drainage equation, J. Phys.: Condens. Matter **8**, 3715 (1996).
[27] S. A. Koehler, S. Hilgenfeldt, and H. A. Stone, Liquid Flow Through Aqueous Foams: The Node-Dominated Foam Drainage Equation, Phys. Rev. Lett. **82**, 4232 (1999).
[28] V. Carrier, S. Destouesse, and A. Colin, Foam drainage: A film contribution? Phys. Rev. E **65**, 061404 (2002).

[29] K. Feitosa, S. Marze, A. Saint-Jalmes, and D. J. Durian, Electrical conductivity of dispersions: From dry foams to dilute suspensions, J. Phys.: Condens. Matter **17**, 6301 (2005).
[30] J. C. Maxwell, *A Treatise on Electricity and Magnetism* (Clarendon, Oxford, 1892), Vol. 1.
[31] R. Lemlich, A theory for the limiting conductivity of polyhedral foam at low density, J. Colloid Interface Sci. **64**, 107 (1978).
[32] M. Dietzel and S. Hardt, Flow and streaming potential of an electrolyte in a channel with an axial temperature gradient, J. Fluid Mech. **813**, 1060 (2017).
[33] J. L. Anderson, Colloid transport by interfacial forces, Annu. Rev. Fluid Mech. **21**, 61 (1989).
[34] R. J. Hunter, *Foundations of Colloid Science*, 2nd ed. (Oxford University Press, Oxford, 2001).
[35] O. Bonhomme, B. Blanc, L. Joly, C. Ybert, and A.-L. Biance, Electrokinetic transport in liquid foams, Adv. Colloid Interface Sci. **247**, 477 (2017).
[36] O. A. Kasperskii and A. F. Sharovarnikov, Influence of electric field on contact interaction of model foam films, Colloid J. USSR **44**, 211 (1982).
[37] A. F. Sharovarnikov and V. N. Tsap, Electroosmotic transport of liquid in foams, Colloid J. USSR **44**, 670 (1982).
[38] A. F. Sharovarnikov, Electrokinetic properties of foams, Colloid J. USSR **46**, 77 (1984).
[39] M. E. Darbello Zaniquelli and F. Galembeck, Modification of foam drainage by electroosmotic effect, Langmuir **1**, 647 (1985).
[40] S. Sett, R. P. Sahu, S. Sinha-Ray, and A. L. Yarin, Experimental investigation of eletrokinetic stabilization of gravitational drainage of ionic surfactants films, Electrochim. Acta **187**, 693 (2016).
[41] O. Bonhomme, O. Liot, A.-L. Biance, and L. Bocquet, Soft Nanofluidic Transport in a Soap Film, Phys. Rev. Lett. **110**, 054502 (2013).
[42] A. H. Sheik, H. C. H. Bandulasena, V. Starov, and A. Trybala, Electroosmotic flow measurements in a freely suspended liquid film: Experiments and numerical simulations, Electrophoresis **38**, 2554 (2017).
[43] A. Hussein Sheik, A. Trybala, V. Starov, and H. C. H. Bandulasena, Electroosmotic flow in free liquid films: Understanding flow in foam plateau borders, Colloids Interfaces **2**, 8 (2018).
[44] F. Johansson and K. L. Kuhlman, mpmath documentation, Numerical calculus, Numerical inverse Laplace transform, Talbot's method from PYTHON version 3.2, mpmath package version 1.0, 2017, available at http://mpmath.org/doc/current/calculus/inverselaplace.html.
[45] D. J. Durian, D. A. Weitz, and D. J. Pine, Scaling behavior in shaving cream, Phys. Rev. A **44**, 7902(R) (1991).
[46] A.-L. Biance, A. Delbos, and O. Pitois, How Topological Rearrangements and Liquid Fraction Control Liquid foam Stability, Phys. Rev. Lett. **106**, 068301 (2011).